

Fig. 2 (CP V ARI RS concrete with addition silica fume) shows in detail the fractured aggregate.

In Fig. 3 (mortar of a concrete composed of CP V ARI Plus at 1 day with 10% silica fume), microstructure is very dense despite its age. Fig. 3 also indicates the formation of a large C-S-H amount, revealing silica action within the matrix even at an early age. A conglomerate of active silica with very well defined form is evident. At this age, the greater the intensity of the curing process, the greater the hydration progress and the better the quality of the final structure, specially if samples are cured under water.

This fact can be confirmed by observing the results obtained for mercury intrusion in CP V ARI Plus paste at 3 and 28 days, as evidenced in Tables 6 and 7. A great reduction in total porosity is observed: The smaller the W/C, the higher the reduction produced.

Fig. 4 (CP V ARI Plus concrete at 1 day without silica fume) shows a void filled with hydrated products and presenting a 0.38mm diameter, characterizing the macropores which can be present in the structure, whether introduced accidentally or deliberately Fig. 4- also reveals that around this isolated pore, the matrix is very dense and compact.

Fig. 5 to 7 present the microstructure of concrete prepared with CP V ARI Plus without silica fume, after 1 day. Fig. 6 shows plates of calcium hydroxide and pore presence within the matrix. Fig. 7 is an enlargement of region 1, showing details of CH plates, with a very well defined form, interspersed with empty spaces characterizing capillary pores.

Fig. 8 (CP V ARI Plus concrete with silica) shows formation of hydrated compounds over the aggregate. The matrix is compact as shown in Fig. 8b.

Fig. 9 (CP V ARI Plus concrete with silica fume) is an enlargement of Fig. 8 showing hydration products (C-H-S and CH) around the aggregates. Fig. 9a presents a conglomerate of hydration products deposited over the aggregate.

Fig. 9b presents various hydration products (CH-Calcium Hydroxide, CSH, OPH – other hydrate products including CSH and Aggregate). It

further shows, in the lower part of 9b, elimination of the transition zone through CSH formation, making it more compact. Here the separation of hydrated products and aggregates is not visible (indicated by the arrow).

Fig. 10a (CP V ARI Plus concrete without silica fume at 28 days) shows the presence of large pores. In Fig. 10 b (CP V ARI Plus concrete without silica fume) a detail appears of a large crack present within the matrix.

Fig. 11a and 11b show a typical image of a paste CP V ARI RS sample without silica fume at 28 days. CH crystals are shown associated with C-S-H type 1. The Ca/Si ratio is 1.70.

Fig. 12 (CP V ARI RS concrete) shows C-S-H formation inside a pore (diameter = 18 $\mu$ m) and a microcrack going through the pores.

Fig. 13a – (CP V ARI RS concrete) shows lack of fibrous crystals inside pores (on the left), and formation of plates inside other pores (on the right), characteristic of the monosulfoaluminate phase (Afm), as indicated by details in Fig. 13b, which is an enlargement of Fig. 13a.

Fig. 14 and 15 present the morphological characteristics and the Ca/Si ratio of the slag particles, in anhydrous form and in a hydrated cement paste.

## CONCLUSIONS

There is an improvement in the microstructure of the concrete when silica fume is used. Pore volume in the paste is reduced, too, even when a low w/c is used.

The filler and pozzolanic effects produce a refinement in the porous structure and change morphology and phase distribution.

Silica fume and slag decrease and/or modify CH crystals forms.

The SEM results showed much greater efficiency in characterizing phases and also changes and improvement occurring in the microstructure for all cements.

Those images reveal the change in characteristics of CH crystals, the more homogeneous and denser interface zone, and the synergy between the slag - silica fume – cement systems.

### ACKNOWLEDGEMENT

Thanks are due to FAPESP, for financing part of the researches. We are grateful to Holdercin Groups S/A and Sika, also to Microsilica - Tecnologia Indústria e Comércio Ltda - for support and for donation of materials as well as pertinent information.

### REFERENCES

1. Mindess, S. Relationship between strength and microstructure for cement based materials: an overview. In: Proceedings of the materials research society, edited: J. F. Young, 1984, p. 53-68.
2. Banthia, N. & Mindess, S. Water permeability of cement paste. - Cement Concrete Research, vol. 19, 1989, p. 727-736.
3. Detwiler, R. J. & Mehta, P. K. Chemical and physical effects of silica fume on the mechanical behavior of concrete. Journal ACI Materials, vol. 86, 1989, p. 609-614.
4. Detwiler, R. J. (1990) Subcritical crack growth in the cement paste steel transition zone. Cement Concrete Research, vol. 20, p. 277-284.
5. Mehta, P. K. Influence of Microstructure of concrete on Durability. In: Conference in Tribute to Micheline Morenville Regourd - Importance of Recent Microstructural Developments in Cement and Concrete. Sherbrooke (Québec) Canada, 6 October 1994.
6. Bentz, D. P. Three-dimensional computer simulation of portland cement hydration and microstructure development. Submitted to Journal of the American Ceramic Society, 1996.
7. Bentz, D. P., Hwang, J.T.G., Hagwood, C., Garboczi, E.J., Snyder, K.<sup>a</sup>, Buenfeld, N., Scrivener, K.L., "Interfacial Zone Percolation in Concrete: Effects of Interfacial Zone Thickness and Aggregate Shape," Materials Research Society, fall, 1994.
8. Silva, I. J. Contribuição ao estudo dos concretos de alto desempenho: propriedades mecânicas, durabilidade e microestrutura.

- EESC, IFSC, IQSC – Interunidades em Ciência e Engenharia de Materiais – USP - São Carlos (Tese de Doutorado), 2000.
9. Sarkar, S. L. & Aitcin, P., C. Dissolution rate of silica fume in very high strength concrete. *Cement and Concrete Research*, vol. 17, 1987, pp. 591-601.
10. Sarkar, S. Aitcin, P. C. & Djellouli, H. Synergistic roles of slag and silica fume in very high-strength concrete. *Cement, Concrete and Aggregates*, vol. 12, N.º 1. Summer 1990, pp. 800-808.
11. Glasser, F. P. Chemical, mineralogical and microstructural changes occurring in hydrated slag-cement blends. In: *Material science of concrete II*, 1991.
12. Camarini, G. Desempenho de misturas de cimento Portland comum e escória de alto-forno submetidas à cura térmica. Tese doutorado, Escola Politécnica da USP, São Paulo, 1995.
13. Li, Y., Langan, B. W. & Ward, M. A. The strength and microstructure of high-strength paste containing silica fume. *Cement, concrete and Aggregates*, vol. 18, N.º 2, 1996, pp. 112-117.
14. Bentz, D. P. & Stutzman, P. E. Evolution of porosity and calcium hydroxide in laboratory concretes containing silica fume. *Cement and Concrete Research*, vol. 24, N.º 6, 1994, pp. 1044-1050.
15. Cao, Y. & Detwiler, R. J. Backscattered electron imaging of cement pastes cured at elevated temperatures. *Cement and Concrete Research*, Vol. 25, N.º 3, 1995, pp. 627-638.
16. Melo, A. B. de "Influência da cura térmica (vapor) sob pressão atmosférica no desenvolvimento da microestrutura dos concretos de cimento Portland" – EESC, IFSC, IQSC – Interunidades em Ciência e Engenharia de Materiais – USP - São Carlos (Tese de Doutorado), 2000.
17. Scrivener, K. & Lewis, M. A microstructure and microanalytical study of heat cured mortars and delayed ettringite formation. Proceedings: 10<sup>th</sup> International Congress on the Chemistry of Cement, Vol. 4 Performance and Durability of Cementitious Materials, Gothenburg, Sweden, 1997.

Table 1 – Clinker and Additions Chemical Properties.

Oxides	Clinker %	Calcário* %	Slag %	Silica Fume %
PF	0,37	42,43	0,92	3,14
SiO <sub>2</sub>	21,09	1,33	34,31	94,3
Al <sub>2</sub> O <sub>3</sub>	5,62	0,40	11,48	0,09
Fe <sub>2</sub> O <sub>3</sub>	3,44	0,26	0,91	0,10
CaO	67,24	54,46	43,39	0,30
MgO	0,66	0,34	6,84	0,43
SO <sub>3</sub>	0,58	0,25	0,90	-.-
K <sub>2</sub> O	0,76	0,05	0,35	0,83
Na <sub>2</sub> O	0,03	0,10	0,16	0,27
Blaine = 470m <sup>2</sup> /kg			BET = 18m <sup>2</sup> /g	

Table 2 - Cement Chemical Properties.

Proportion	CP V ARI RS %	CP V ARI Plus %
Clinker	60,4	90,33
Slag	29,61	-
Calcium Sulfate	4,91	4,45
Calcareous Filler	5,08	5,22
C <sub>3</sub> S	38,26	58,95
C <sub>2</sub> S	7,66	10,15
C <sub>3</sub> A	4,92	7,36
C <sub>4</sub> AF	6,32	9,46

Table 3 - Mixture proportions to produce a slump of 120mm ± 20mm.

Mixture proportions (MP)	Theoretical consumption of materials for m <sup>3</sup> of concrete (kg)							
	Cement	Silica Fume	SP	Water	Sand	crushed 1	crushed 2	Total crushed
1:1,2:2:0,3	513	57,0	9,1	171	684	456	684	1140
1:1,2:2:0,3	570	-.-.-	8,5	171	684	456	684	1140
1:1,82:2,82:0,4	388	42,0	6,9	168	764	474	710	1184
1:1,82:2,82:0,4	420	-.-.-	6,3	168	764	474	710	1184
1:2,75:3,75:0,5	286	32	5,7	159	874	477	715	1192
1:2,75:3,75:0,5	318	-.-.-	5,0	159	874	477	715	1192

Table 4 - Compressive Strength of concretes produced with CP V ARI Plus, with or without silica fume.

Mixture proportions		MPa									
	1:m	W/C	f <sub>cj1</sub>	f <sub>cj3</sub>	f <sub>cj7</sub>	f <sub>cj14</sub>	f <sub>cj21</sub>	f <sub>cj28</sub>	f <sub>cj63</sub>	f <sub>cj91</sub>	f <sub>cj365</sub>
<b>Without</b>	1:3,2	0,3	<b>53,5</b>	64,9	<b>71,6</b>	73,3	78,3	<b>81,4</b>	88,9	95,6	<b>97,6</b>
<b>Silica</b>	1:4,6	0,4	<b>36,9</b>	45,1	<b>51,2</b>	60,4	62,7	<b>67,4</b>	71,5	77,6	<b>81,1</b>
<b>Fume</b>	1:6,5	0,5	<b>21,8</b>	34,1	<b>40,9</b>	49,0	51,9	<b>54,0</b>	57,9	59,5	<b>61,9</b>
<b>With</b>	1:3,2	0,3	<b>55,2</b>	70,3	<b>76,0</b>	82,5	85,1	<b>88,9</b>	95,3	102,6	<b>105,1</b>
<b>Silica</b>	1:4,6	0,4	<b>38,6</b>	50,2	<b>59,1</b>	64,7	66,7	<b>72,0</b>	76,0	82,1	<b>84,7</b>
<b>Fume</b>	1:6,5	0,5	<b>23,5</b>	38,0	<b>46,7</b>	54,6	57,3	<b>59,1</b>	64,5	66,3	<b>67,1</b>

Table 5 - Compressive Strength of concretes produced with CP V ARI RS, with or without silica fume.

Mixture proportions		MPa									
	W/C	f <sub>cj1</sub>	f <sub>cj3</sub>	f <sub>cj7</sub>	f <sub>cj14</sub>	f <sub>cj21</sub>	f <sub>cj28</sub>	f <sub>cj63</sub>	f <sub>cj91</sub>	f <sub>cj365</sub>	
<b>Without</b>	1:3,2	0,3	<b>31,9</b>	48,3	<b>60,5</b>	68,8	76,4	<b>79,1</b>	86,7	93,5	<b>98,2</b>
<b>Silica</b>	1:4,6	0,4	<b>23,2</b>	31,9	<b>43,5</b>	46,9	52,9	<b>57,1</b>	64,6	71,6	<b>74,9</b>
<b>Fume</b>	1:6,5	0,5	<b>15,5</b>	25,8	<b>37,3</b>	43,5	47,9	<b>50,1</b>	55,3	58,3	<b>62,9</b>
<b>With</b>	1:3,2	0,3	<b>38,2</b>	61,2	<b>72,9</b>	75,8	82,5	<b>88,7</b>	97,7	105,1	<b>109,1</b>
<b>Silica</b>	1:4,6	0,4	<b>24,9</b>	38,2	<b>53,4</b>	60,6	64,7	<b>68,2</b>	77,7	85,5	<b>88,1</b>
<b>Fume</b>	1:6,5	0,5	<b>16,7</b>	30,7	<b>43,9</b>	48,6	54,4	<b>56,7</b>	63,2	69,3	<b>70,1</b>

Table 6 - Properties of concretes at 28 days - CP V ARI Plus.

Properties of Pastes and Concretes - CP V ARI Plus							$\alpha_{28}$ - % hydration at 3 days	
		Total Porosity (%)						
Mixture proportions		Mechanical Properties		Concrete	Paste			
	W/C	$f_{cj28}$ (MPa)	$E_{cj28}$ (GPa)	28 days	3 days	28 days		
Without Silica	1:3,2 0,3	81,4	49,1	<b>10,12</b>	1:0,3	20,81	<b>16,12</b>	<b>62,8</b>
Silica	1:4,6 0,4	67,4	41,1	<b>11,00</b>	1:0,4	23,61	<b>19,55</b>	<b>77,9</b>
Fume	1:6,5 0,5	54,0	27,5	<b>13,16</b>	1:0,5	31,88	<b>22,19</b>	<b>72,9</b>
With Silica	1:3,2 0,3	88,9	54,2	<b>7,19</b>	1:0,3	15,87	<b>12,08</b>	<b>55,1</b>
Silica	1:4,6 0,4	72,0	46,3	<b>8,45</b>	1:0,4	22,23	<b>15,68</b>	<b>69,9</b>
Fume	1:6,5 0,5	59,1	32,1	9,82	1:0,5	27,04	<b>20,71</b>	<b>68,5</b>

Table 7 - Properties of concretes at 28 days - CP V ARI RS.

Properties of Pastes and Concretes - CP V ARI RS							$\alpha_{28}$ - % hydration at 3 days.	
		Total Porosity (%)						
Mixture proportions		Mechanical Properties		Concrete	Paste			
	W/C	$f_{cj28}$ (MPa)	$E_{cj28}$ (GPa)	28 days	3 days	28 days		
Without Silica	1:3,2 0,3	79,1	48,6	10,12	1:0,3	20,81	<b>16,12</b>	<b>54,2</b>
Silica	1:4,6 0,4	57,1	40,3	11,00	1:0,4	23,61	<b>19,55</b>	<b>76,9</b>
Fume	1:6,5 0,5	50,1	29,3	13,16	1:0,5	31,88	<b>22,19</b>	<b>78,3</b>
With Silica	1:3,2 0,3	88,7	52,3	7,19	1:0,3	15,87	<b>12,08</b>	<b>48,7</b>
Silica	1:4,6 0,4	68,2	44,5	8,45	1:0,4	22,23	<b>15,68</b>	<b>61,4</b>
Fume	1:6,5 0,5	56,7	33,0	9,82	1:0,5	27,04	<b>20,71</b>	<b>68,7</b>

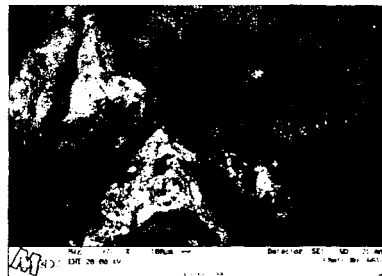


Fig. 1a - Concrete CP V ARI Plus without silica fume.

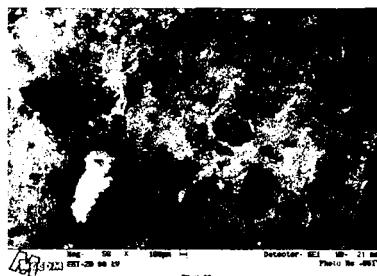


Fig. 1b - Concrete CP V ARI Plus with silica fume.

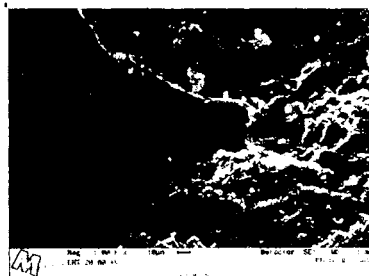


Fig. 2 - Concrete with CP V ARI RS and silica fume. Fractured aggregate and interface region.

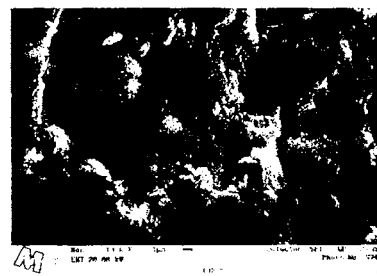


Fig. 3 - Mortar of a concrete CP V ARI Plus at 1 day,  $w/c=0.3$ .

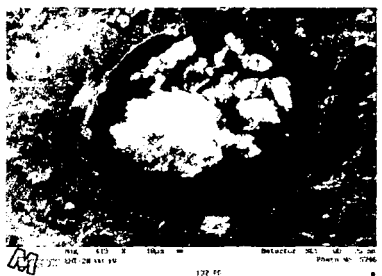


Fig. 4 - Concrete CP V ARI Plus without silica fume, 1 day. Air void filled with hydration products.

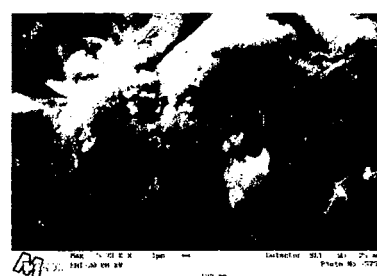


Fig. 5 - concrete CP V ARI Plus without silica fume, 1 day.

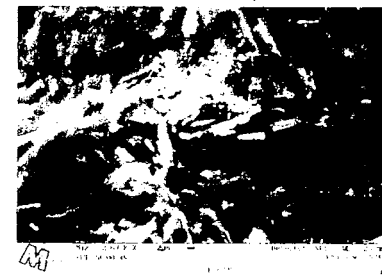


Fig. 6 - mortar CP V ARI Plus with addition of silica fume. Calcium hydroxide plates, 1 day.

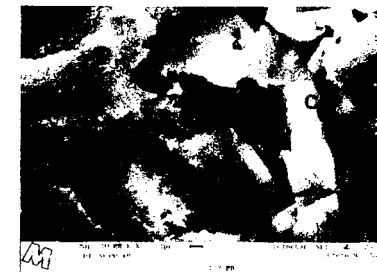


Fig. 7 - Enlargement of point 1 from Fig. 6 – calcium hydroxide plate.

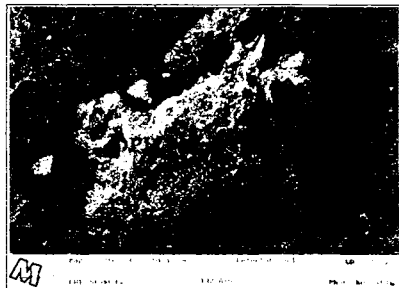


Fig. 8a – mortar sample of concrete CP V ARI Plus with silica fume. Formation of hydrated compound over the aggregate area.

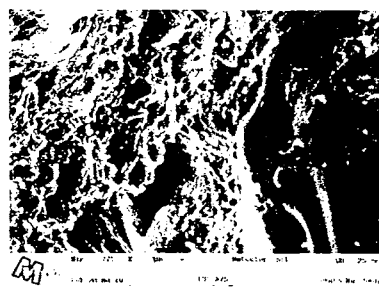


Fig. 8b – Enlargement of Fig. 8a, where a very compact matrix is observed, without emptiness or capillary porosity in the paste aggregate interface zone.

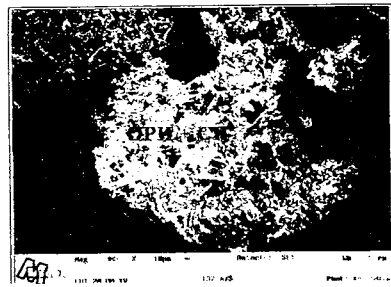


Fig. 9a - mortar sample of CP V ARI Plus with silica fume. Detail of hydration products around the aggregate (enlargement of Fig. 8)

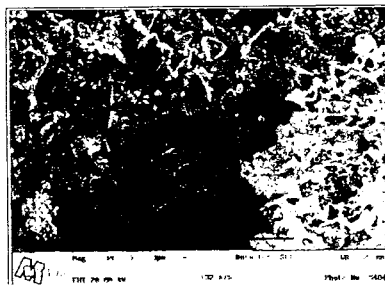


Fig. 9b - Enlargement of Fig. 9a, where elimination of the transition between the aggregate and the matrix.

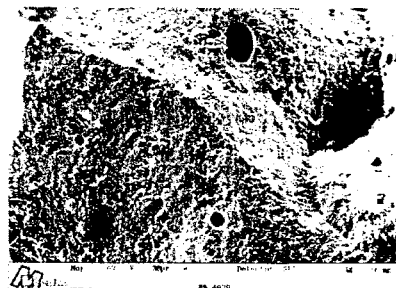


Fig. 10a - concrete (1:4.64) CP V ARI Plus without silica fume, shows texture Characteristics and presence of pores.

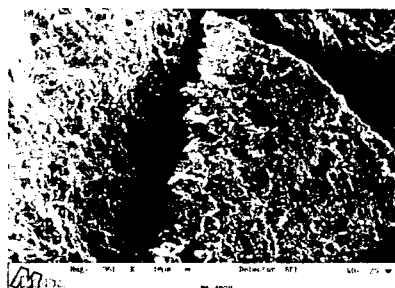


Fig. 10b - concrete CP V ARI Plus without silica fume - presence of large crack in the matrix.

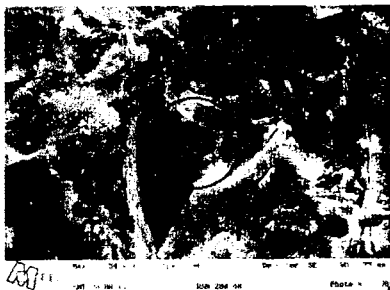


Fig. 11a - paste sample CP V ARI RS without silica fume at 28 days.



Fig. 11b - Enlarged image of the region circled in Fig. 11a – showing CSH.

Point	Phase	Ca/Si	Al/Ca	Ca/(Si+Al)
1	C-S-H	1,70	0,04	1,43

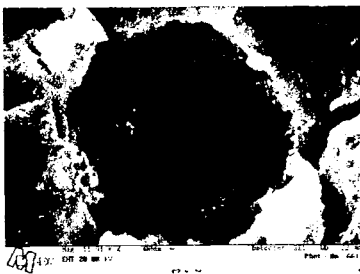


Fig. 12 - concrete CP VARI RS showing the formation of C-S-H inside a pore (diameter=1,8  $\mu\text{m}$ ) with a microcrack.

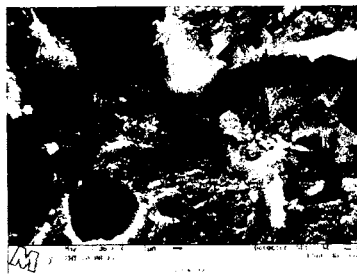


Fig. 13a - Concrete CP V ARI RS. Absence of fibrous crystals inside a pore (to the left) and formation of plates inside another pore. (to the right ).



Fig. 13b – Enlargement of Fig. 13a – detail of the formation of hexagonal plates inside the sample pore, typical arrangement of face-edge connection (Afm).

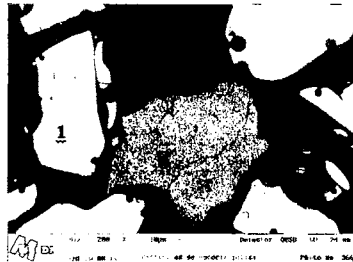


Fig. 14 - Polished slag-grain.

	Ca/Si	Al/Ca	Ca/(Si+Al)
1 Slag	1,58	0,21	1,19

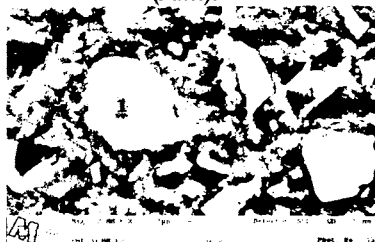


Fig. 15 – Enlargement of a slag particle present in the hardened cement paste. Polished surface.

	Ca/Si	Al/Ca	Ca/(Si+Al)
1 Slag	1,48	0,23	1,11